Available online at www.sciencedirect.com
SCIENCE DIRECT®
Journal of Crystal Growth 270 (2004) 21–29
JOURNAL OF CRYSTAL GROWTH
www.elsevier.com/locate/jcrysgro

Properties of high *k* gate dielectric gadolinium oxide deposited on Si (1 0 0) by dual ion beam deposition (DIBD)

Jian-Ping Zhou[a,*], Chun-Lin Chai[a], Shao-Yan Yang[a], Zhi-Kai Liu[a], Shu-Lin Song[a], Yan-Li Li[a], Nuo-Fu Chen[a,b]

[a] *Institute of Semiconductors, Chinese Academy of Sciences, Key Laboratory of Semiconductor Materials Science, Beijing 100083, People's Republic of China*

[b] *Institute of Mechanics, Chinese Academy of Sciences, National Microgravity Laboratory of Chinese Academy of Sciences, Beijing 100080, People's Republic of China*

Received 24 April 2004; accepted 27 May 2004

Available online 28 July 2004

Communicated by M. Schieber

Abstract

Gadolinium oxide thin films have been prepared on silicon (1 0 0) substrates with a low-energy dual ion-beam epitaxial technique. Substrate temperature was an important factor to affect the crystal structures and textures in an ion energy range of 100–500 eV. The films had a monoclinic Gd_2O_3 structure with preferred orientation ($\bar{4}$ 0 2) at low substrate temperatures. When the substrate temperature was increased, the orientation turned to (2 0 2), and finally, the cubic structure appeared at the substrate temperature of 700°C, which disagreed with the previous report because of the ion energy. The AES studies found that Gadolinium oxide shared Gd_2O_3 structures, although there were a lot of oxygen deficiencies in the films, and the XPS results confirmed this. AFM was also used to investigate the surface images of the samples. Finally, the electrical properties were presented.

PACS: 77.84.−s; 81.15.Hi; 61.10.−i; 39.25+k; 82.80.Pv

Keywords: A1. Auger electron spectroscopy; A1. Atomic force microscopy; A1. Crystal structures; A1. X-ray photoelectron spectroscopy; A3. Ion-beam deposition; B1. Oxides

1. Introduction

In the past decades, astounding progress has been made in semiconductor technology, achieved through continual scaling-down silicon devices. The silicon technology is in the dominant status, because of its reaction with oxygen in a controlled

*Corresponding author. Department of Materials Science and Engineering, Tsinghua University, State Key laboratory of New Ceramics and Fine Processing, Beijing 100084, China..

E-mail addresses: zhoujp@mail.tsinghua.edu.cn, j_p_zhou@sina.com (J.-P. Zhou).

0022-0248/$ - see front matter © 2004 Elsevier B.V. All rights reserved.
doi:10.1016/j.jcrysgro.2004.05.114

manner to form superb insulators excellent mechanical, dielectric and electrical properties. The dielectrics are used in the silicon semiconductor industry as the transistor gate dielectric in metal–oxide–semiconductor field-effect transistor (MOSFET) logic devices, which is the basic microelectronics device in chips. Because the thickness of the gate dielectric must reduce with the decrease of the gate length, a major challenge that needs to be overcome in scaling the MOS transistor is the thickness of the silicon dioxide insulator. Tunneling-induced leakage currents and dielectric breakdown will lead to unacceptable device performance for oxide thickness below ~ 1.5 nm [1]. Therefore, a high dielectric-constant material is needed to replace SiO_2 as the gate dielectric. The substitute meets some challenging requirements in order to achieve performance comparable to silicon oxide. These requirements include dielectric constant, band gap, band alignment to silicon, low oxygen diffusivity, lower leakage current than SiO_2 at an equivalent oxide thickness (t_{eq} defined as $(k_{SiO_2}/k_{oxide})t_{phys}$) less than 1.5 nm, thermodynamic stability in contact with silicon at temperature exceeding 800°C, high-quality interface with silicon with low interfacial state density [2]. Some binary metal oxides are currently under consideration as the potential replacements for SiO_2 as the gate dielectrics, such as Ta_2O_5 [3,4], TiO_2 [5], ZrO_2 [6].

The rare earth oxides are attractive candidates based on thermodynamic energy considerations [7] and a high conduction band offset over 2 eV [8]. Among several binary earth metal oxides under consideration, Gadolinium sesquioxide, one of the promising substitutes for SiO_2 in ultra-large-scale integration (ULSI), has attracted much attention recently. It has a band gap of 5.3 eV [9,10], and a high dielectric constant of 14–20 [11,12], meaning that a 4.9 nm film can satisfy the requirement of a 1 nm equivalent oxide thickness. Another interesting topic on studying Gadolinium oxide is its structures. Gd_2O_3 is the only stable oxide reported in gadolinium oxide [13]. It occurs in three crystal forms A-, B-, and C-forms. The A-type is hexagonal, the B-type is a monoclinic distortion of the A-form while the C-form structure shares an isomorphic cubic Mn_2O_3 structure [14]. The A-form structure is stable at high temperature, and the C-form is stable at room temperature while B-form is stable in a temperature domain higher than room temperature [15]. Additionally, the cubic Gd_2O_3 has one of the closest lattice-matches to silicon, resulting from the fact that the cubic Gd_2O_3 lattice (10.812 Å) is nearly twice as that of the silicon (5.43 Å). Its lattice mismatch with Si(1 0 0) surface is within 0.5%. Thus, a cube-on-cube epitaxy between a Gd_2O_3 (1 0 0)-oriented crystal and the Si(1 0 0) surface is expected.

In this paper, we study the properties of gadolinium oxide prepared by a low-energy dual ion-beam deposition (DIBD) technique.

2. Experimental procedure

Gadolinium oxide thin films have been prepared by a low-energy DIBD technique. The gadolinium ions and oxygen ions were generated with a Bernas and a Freeman ion source chamber, respectively. Two independent mass-selected ion beams were designed to select the interesting ion species, which were alternately merged into the target to facilitate compound formation. The ion energy can be set as low as 50 eV to reduce self-sputtering and lattice damage of the deposition film [16,17].

Phosphor-doped silicon (1 0 0) wafers were used as substrates. The wafers were cleaned with ethanol, acetone, HF and deionized water and then delivered into the deposition chamber by a mechanical hand. The vacuum in the chamber was kept less than 1×10^{-6} Pa all the while. Through mass-selection in the magnetic field and acceleration in the electric field, the ion beams were alternately deposited on the substrate. The Gd^+ and O^+ ion current was around 30 and 150 μA, respectively.

The samples were deposited at different conditions as shown in Table 1.

The crystal structures of the as-deposited films were analyzed by X-ray diffraction (XRD). The surface properties were characterized by Ex situ Atomic Force Microscopy (AFM). The PHI-610/SAM AES (Auger Electron Spectroscopy) system was employed for analyzing the composition of the films and the MK II XPS (X-ray Photoelectron Spectroscopy) for the chemical analysis.

Table 1
The deposited conditions and characters of the samples

Sample	A	B	C	D	E	F
Ion energy	100 eV	300 eV	300 eV	500 eV	300 eV	100 eV
Substrate temperature	300°C	300°C	500°C	500°C	700°C	500°C, in situ anneal at 800°C for 30 min
Total dose of O^+/Gd^+	$4\times10^{17}\,cm^{-2}/1\times10^{17}\,cm^{-2}$	$4\times10^{17}\,cm^{-2}/1\times10^{17}\,cm^{-2}$	$4\times10^{17}\,cm^{-2}/1\times10^{17}\,cm^{-2}$	$4\times10^{17}\,cm^{-2}/1\times10^{17}\,cm^{-2}$	$5\times10^{17}\,cm^{-2}/1\times10^{17}\,cm^{-2}$	$5\times10^{17}\,cm^{-2}/1\times10^{17}\,cm^{-2}$
Structures	Monoclinic ($\bar{4}\,0\,2$)	Monoclinic ($\bar{4}\,0\,2$)	Monoclinic (2 0 2)	Monoclinic (2 0 2)	Monoclinic (2 0 2) and cubic (2 2 2)	Cubic (2 2 2) and monoclinic ($\bar{4}\,0\,2$)
Grain size (nm)	15.4 ($D_{\bar{4}02}$)	10.8 ($D_{\bar{4}02}$)	26 (D_{202})	24 (D_{202})	36 (D_{202})	15.1 (D_{202}) 14.3 ($D_{\bar{4}02}$)
Roughness	2.43 nm	3.487 nm	5.19 nm	2.967 nm	0.976 nm	0.444 nm

3. Results and discussion

3.1. Structural analyses

XRD patterns for the samples have been measured and were shown in Fig. 1. The typical results were comparatively listed in Table 1. At low substrate temperature of 300°C, sample A and sample B share the same B-form structure with the ($\bar{4}\,0\,2$) preferred orientation although their deposited ion energy is different. When the substrate temperature is increased to 500°C, sample C and sample D have the similar results but the preferred orientation turn to (2 0 2). When the substrate temperature is 700°C, cubic (2 2 2) peak appears. This means the substrate temperature is an important factor to affect the preferred orientation of the film in comparison to the ion energy. Sample F was designed to confirm this idea. The sample was grown with ion energy of 100 eV at temperature of 500°C, and then was in situ annealed at temperature of 800°C for 30 min into the mixed phases of B-form structure with ($\bar{4}\,0\,2$) orientation and C-form structure with (2 2 2) orientation. The substrate temperature can change the structures and the preferred orientation. But these disagree with the polymorphic transformation [14,15], where the cubic structure appears at low temperature while the monoclinic structure appears at high temperature. Other work groups also obtained the cubic structure at a temperature range of 200–550°C [18,19].

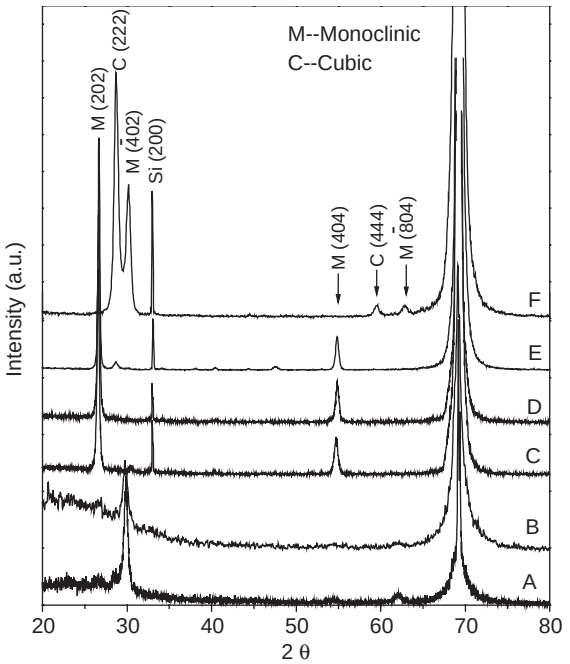

Fig. 1. XRD patterns of Gd_2O_3 films for various preparing conditions.

The fact that the B-form structure of gadolinium oxide appears at low substrate temperature may be owing to ion bombards. When a low-energy ion beam bombards a solid, a series of complex interactions occurs by which the primary ions transfer a part of their energy to the solid. As a result of this perturbation, the solid emits photons

and electrons, as well as atomic and molecular ions and neutrals. In the energy range considered here (50–500 eV), the primary ions do not penetrate deeply into the solid and they lose energy mainly during discrete elastic collisions with the target atomic nuclei. This results in the epitaxial growth of the film. During the deposition, the ions have much more energy than the thermal energy (the ion energy with 1 eV is equivalent to the thermal energy of its corresponding neutral particle at about 10^4 K), resulting in the high ion chemical activity and heating up at a local area. Then it is easy to understand that monoclinic structure formed at a low substrate temperature. Sample E has higher substrate temperature while preparing and sample F has been annealed at 800°C in situ, then both samples were cooled down at a low speed in the vacuum chamber. Cubic structure gadolinium oxide was formed in the two samples. The low-energy dual ion-beam deposition can prepared some anomalous structures that the other common technology cannot achieve.

The grain size in the preferring direction was obtained by Scherrer formula

$$\beta_{\mathrm{m}} = \frac{K\lambda}{D\cos\theta},$$

where β_{m} = FWHM (full-width at half-maximum), $K = 0.89$ a constant and D is the grain size at HKL direction, which was listed in Table 1. With the substrate increasing, the grain size was growing lager, but in sample F, the two phases impeded grain growth each other, resulting in a smaller size.

The relative integrated intensity of the peaks can be calculated by [20]

$$R = \left(\frac{1}{V^2}\right)\left[|F_{hkl}|^2 P\left(\frac{1+\cos^2 2\theta}{\sin^2\theta\cos\theta}\right)\right]e^{-2M}, \qquad (1)$$

where R is the theoretical integrated intensity, V the volume of unit cell, F the structure factor, P the multiplicity, $(1+\cos^2 2\theta/\sin^2\theta\cos\theta)$ = Lorentz-polarization factor, and e^{-2M} is the temperature factor.

This fomula was applicable when crystallites were randomly oriented in the powder samples, but in the films, the integrated intensity was affected by the preferential orientation of the crystal growth. It could eliminate the influence of preferential orientation to determine the volume fraction of different phases by normalizing the experimental intensity [21,22].

In the process of powder analysis, the thickness of the sample is commonly more than the X-ray penetration depth, thus the volume of the part sample tested is constant. But in films, the thickness of the sample is often less than the depth of X-ray penetration. The influence of thickness on the integrated intensity of the peaks should be considered.

When X-ray get to the surface of the film with angle θ as shown in Fig. 2, in which D_{F} is the thickness of the film while D_{P} the depth of X-ray penetration, the area in the surface of the film exposed is $S/\sin\theta$, where S is the cross-sectional area of the light. Considering the thickness of the film, the volume tested is written

$$V = \frac{SD_{\mathrm{F}}}{\sin\theta}. \qquad (2)$$

The physical process is very complex when X-ray irradiates on the materials. Summing up the all factors affecting the intensity of XRD, the integrated intensity of peaks was written

$$I = I_0\frac{\lambda^3}{32\pi R}\left(\frac{e^2}{mc^2}\right)^2\frac{|F_{hkl}|^2}{V_{\mathrm{c}}^2} P\frac{1+\cos^2 2\theta}{\sin^2\theta\cos\theta}A(\theta)e^{-2M}\,\mathrm{d}V, \qquad (3)$$

where I_0 is the intensity of incident X-ray, λ the incident wavelength, $A(\theta)$ the absorption factor, and $\mathrm{d}V = (S/\sin\theta)\mathrm{d}x$.

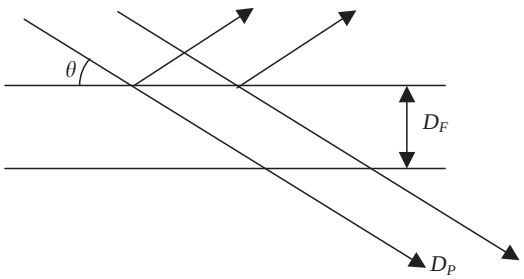

Fig. 2. The X-ray penetration deepness is more than the thickness of the film.

The integral range of dx is $0-D_F$. Then the relative integrated intensity of peaks becomes

$$I \sim \frac{|F_{hkl}|^2}{V_c^2} P \frac{1+\cos^2 2\theta}{\sin^2\theta\cos\theta} \frac{1}{\sin\theta} e^{-2M}. \quad (4)$$

In comparison to Eq. (1), Eq. (4) has an added factor $(1/\sin\theta)$. Then it is easy to understand the experimental intensity ratio between a peak at low angle and its parallel peaks at high angle, for example, between (2 0 2) and (4 0 4), is more than the corresponding ratio in Joint Committee for Powder Diffraction Standards (JCPDS). But if the sample size is less than the cross-sectional area of X-ray beam, Eq. (4) is inapplicable.

3.2. Atomic force microscopy

The surface morphology of the gadolinium oxide films was imaged by AFM. Fig. 3 shows the surface images of samples A–E. The

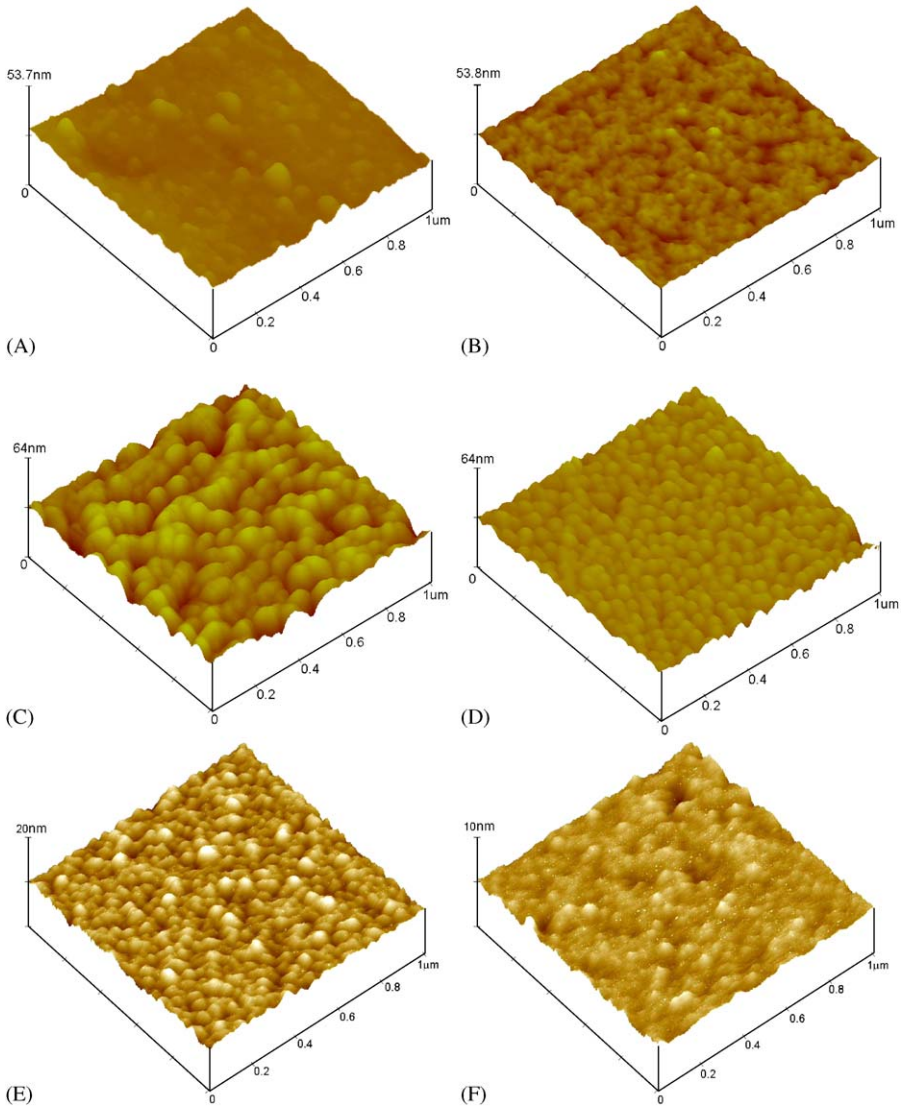

Fig. 3. $1 \times 1\,\mu m$ AFM images of the samples.

root-mean-square (rms) surface roughness of the films was measured and listed in Table 1. The surface of sample A shows a clear pit in size about 250 nm. And on the other sample surfaces, the pits are under 100 nm or even disappear. Sample D has a most uniform surface with a grain size of about 60 nm. The substrate temperature and ion energy are important to affect the surface morphology and its roughness. High substrate temperature is helpful to crystallize.

3.3. AES analyses

The AES system was employed for analyzing the composition of the films. PHI-610/SAM instrument was equipped with a 3 keV electron beam 30° off normal and a cylindrical mirror analyzer in the vacuum of 3.9×10^{-9} Torr. Depth spectra were obtained while sputtering through the films with Ar^+ ions. Fig. 4 shows the Auger differential spectra at the different depth of sample C. There are gadolinium, silicon, carbon and oxygen at the surface of the film, and carbon disappears inside the film.

The concentration ratio of gadolinium and oxide was calculated by the spectra together with the sensitivity factors. To our astonishment, the results show that the ratio of gadolinium and oxygen is not 2:3 but 1:1 at the sample surface and 2:1 inside the film, although the films share Gd_2O_3 structures. This means there are a lot of oxygen deficiencies in the film, to which the luminescent phenomenon was contributed [23]. Sample A, B and D share the similar characters.

3.4. XPS analyses

It is amazed that gadolinium oxides with Gd_2O_3 structures do not have the stoichiometric 2:3. We used the XPS for a more study. The electron spectroscopy for chemical analysis (ESCA) is useful to investigate the changing characterization in the chemical environment of an element in structures. The measurements were performed on

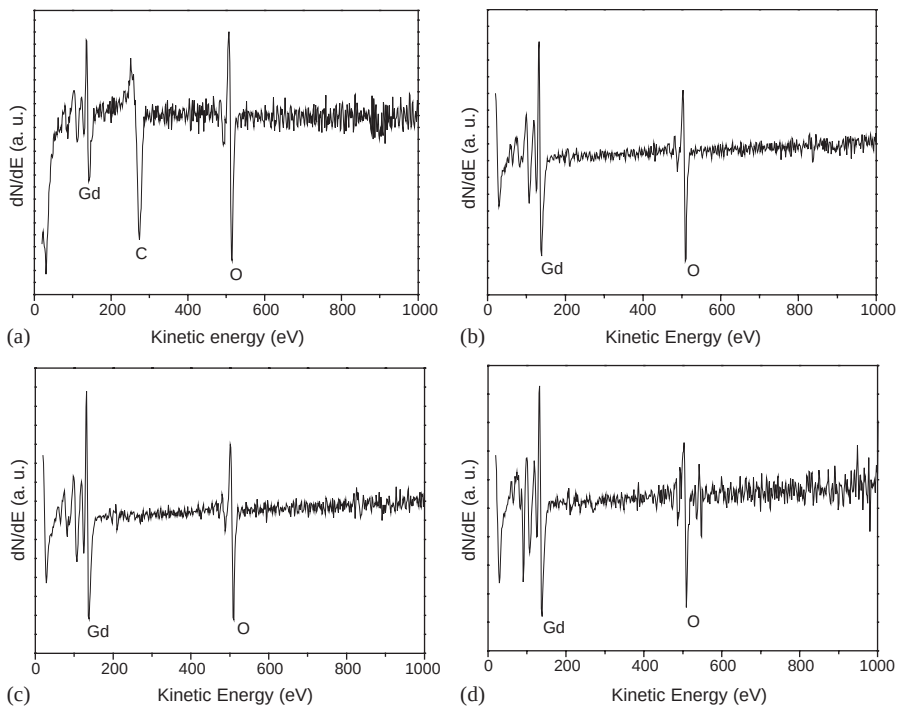

Fig. 4. Auger differential spectra of sample C: (a) at the surface of the sample; (b) at the depth of the sample sputtered for 1.8 min; (c) sputtered for 2.4 min; (d) sputtered for 3.2 min.

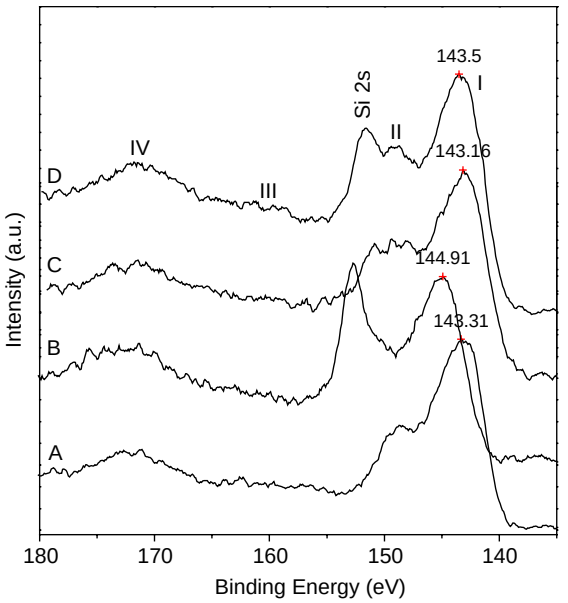

Fig. 5. Gd 4d XPS spectra of sample A–D. The range of $4d_{5/2}$ binding energy is 143.3–144.9 eV.

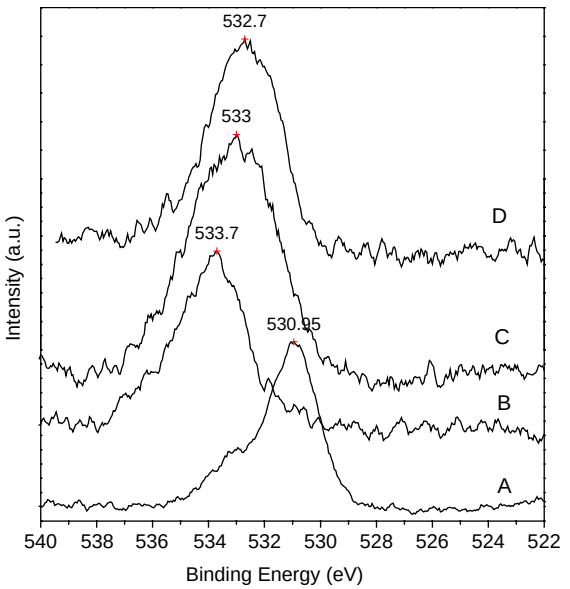

Fig. 6. O1s XPS spectra of sample A–D. The binding energy is in the range of 531–533.7 eV.

an MK II photoelectron spectrometer using Mg Kα radiation (1254 eV) in the vacuum of 2×10^{-9} Torr. Soft sputtering with argon ions was used to obtain a clean surface.

Fig. 5 shows the Gd 4d spectra of the binding energy vs. the intensity for some samples. Their wide spread multiplet structure, caused by the electrostatic interaction between the 4d and 4f shells have been described using an atomic many-particle description by van der Laan [24,25]. Another method of describing core–hole photoemission is the one-electron model with a spin-dependent field [26]. Both methods match the first five peaks with the sublevels of the $\frac{5}{2}$ level very well. The spin-orbit interaction splits the terms into levels with $J = 6, 5, 4, 3, 2$ for ^9D as peak I. The other peaks are assigned differently though they share similar experimental characteristics with the four peaks. In our data, Si 2s spectra appear besides Gd 4d spectra. This is caused by the thin thickness of the films. The binding energy of Gd $4d_{5/2}$ is in the range of 143.3–144.9 eV.

Fig. 6 shows the O 1s spectra of the binding energy vs. the intensity for the corresponding samples. The peaks of binding are in the range of 531–533.7 eV. This is a little larger than the standard binding energy in the metal oxide. On the other hand, this is maybe caused by the shifts of the system. Then we calculated the difference between O 1s and Gd 4d. They are in the range of 387.6–389.8 eV, also a little larger than the difference in the standard spectra [27]. The higher binding energy of O 1s indicates its low electronegativity caused by oxygen deficiencies in the films. This agrees with the AES results.

We increased the dose ratio between the O^+ and Gd^+ ions while preparing samples E and F because of the oxygen deficiencies in the previous films. The two samples were analyzed by XPS and some Gd_2O_3 powder (cubic structure) was analyzed for comparison. Fig. 7 shows the XPS spectra of samples E and F together with the Gd_2O_3 powder. The binding energy of Gd 4d and O 1s decreases in sample E and F in comparison to samples A–D, but the difference between O 1s and Gd 4d increases a little, indicating a higher electronegativity and lower oxygen deficiencies. The Gd 4d spectra of samples and powder share the same shape as the previous samples. However, the binding energy of O 1s in the samples and the

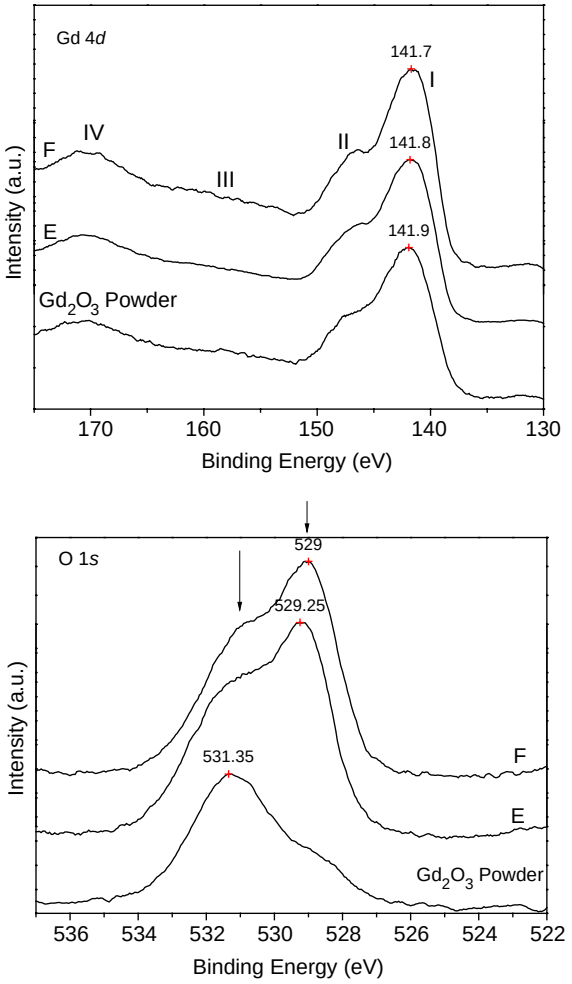

Fig. 7. Gd 4d and O 1s XPS spectra of sample E and F together with Gd_2O_3 powder.

powder splits into two distinctive peaks because of the different oxygen position in the crystal cell. The relative intensity of the two splitting peaks is different between the samples and powder, which maybe caused by the deficiencies in the two samples or the different crystal structure between the samples and powder.

3.5. Electrical properties

Under consideration of structures, surfaces and thickness, the sample D was selected to investigate the electrical properties. Firstly, the sample was

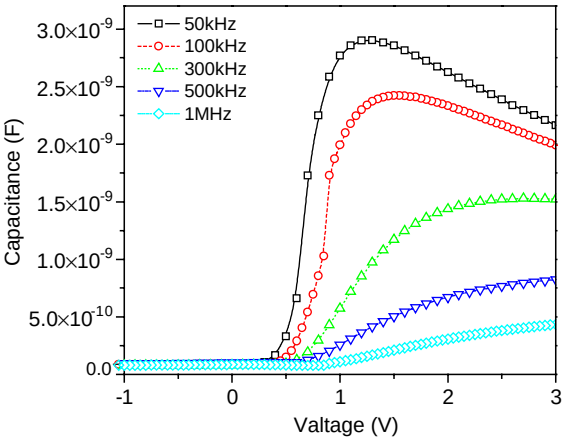

Fig. 8. $C-V$ curves of sample D, deposited at 500°C with ion energy 500 eV and subsequently annealed in an atmosphere of flowing nitrogen at 800°C for 30 min.

annealed in an atmosphere of flowing nitrogen automatically temperature-conditioned annealing furnace at 800°C for 30 min. AuGeNi/Au dots 300 μm in diameter were evaporated onto the oxide surface as electrodes. The other probe was placed on the back of Si substrate evaporated with Al for 600 nm thickness. $C-V$ measurements were performed using a Keithley model-82win simultaneous $C-V$ measurement system.

The capacitance vs. voltage curves for a MOS diode made of a 25.5 nm thick Gd_2O_3 film are shown in Fig. 8. The dielectric constant ε is about 20, which suggest a t_{eq} as low as 5 nm. The flat band capacitance and flat band voltage were 4.1×10^{-7} F/cm^2 and 9.0 V, respectively, which indicate there are high charge density in the oxide, caused by oxygen deficiencies.

4. Conclusion

In summary, we have shown in this work that gadolinium oxide thin films had different crystal structures and textures at different experimental conditions. With the substrate temperature increasing, the monoclinic structure with preferred orientation $(\bar{4}\,0\,2)$ turned to $(2\,0\,2)$ orientation, and finally the mixed phases of monoclinic structure with $(\bar{4}\,0\,2)$ orientation and cubic structure with

(4 0 0) orientation were formed. This does not agree with the previous report because of the heating by the ion energy. AES and XPS showed that there are a lot of oxygen deficiencies in the thin films although the samples shared Gd_2O_3 structures. The flat band voltage is too big for the high charge density caused by the oxygen deficiencies in the oxide. And the dielectric constant of the film is about 20.

Acknowledgements

This work is jointly supported by Special Funds for Major State Basic Research Projects (Grant Nos. G20000365 and G2002CB31905) and the National Natural Science Foundation of China (Grant No. 60176001 and 60206007).

References

[1] P.S. Peercy, Nature 406 (2000) 1023.
[2] G.D. Wilk, R.M. Wallace, J.M. Anthony, Appl. Phys. Lett. 89 (2001) 5243.
[3] Z.-W. Fu, L.-Y. Chen, Qi.-Z. Qin, Thin Solid films 340 (1999) 164.
[4] L.W. Tu, W.C. Kuo, K.H. Lee, P.H. Tsao, C.M. Lai, Appl. Phys. Lett. 77 (2000) 3788.
[5] B.-C. Kang, S.-O. Lee, J.-H. Boo, Surf. Coatings Technol. 131 (2000) 88.
[6] T. Ngal, W.J. Qi, R. Sharma, J. Fretwell, X. Chen, J.C. Lee, S. Banerjee, Appl. Phys. Lett. 76 (2000) 502.
[7] K.J. Hubbard, D.G. Schlom, J. Mater. Res. 11 (1996) 2757.
[8] J. Robertson, J. Vac. Sci. Technol. B 18 (2000) 1785.
[9] S.S. Derbeneva, S.S. Batsano, Dokl. Chem. 175 (1967) 710.
[10] S.S. Batsono, E.V. Dulepov, Sov. Phys. Solid State 7 (1965) 995.
[11] R.D. Shannon, J. Appl. Phys. 73 (1993) 348.
[12] J. Kwo, M. Hong, A.R. Kortan, K.T. Queeney, Y.J. Chabal, J.P. Mannaerts, T. Boone, J.J. Krajewski, A.M. Sergent, J.M. Rosamilia, Appl. Phys. Lett. 77 (2000) 130.
[13] T.B. Massalski, Binary Alloy Phase Diagrams, Vol. 2, the Materials Information Society, (American), Materials Park, OH, ASM, 1990, p. 1905.
[14] R.G. Haire, L. Eyring, Comparisons of the binary oxides, in: K.A. Gschneider Jr., L. Eyring (Eds.), Handbook on the Physics and Chemistry of Rare Earths, Vol. 18. Lanthanides/Actinides: Chemistry, Elsevier Science B. V., Amsterdam, p. 429 (Chapter 125).
[15] C. Boulesteix, Defects and phase transformation near room temperature in rare earth sesquioxides, in: K.A. Gschneider Jr., L. Eyring (Eds.), Handbook on the Physics and Chemistry of Rare Earths, Vol. 5, North-Holland Publishing Company, Amsterdam, 1982, p. 321 (Chapter 44).
[16] Sh.-J. Su, W.-Sh. Jiang, F.-G. Qin, X.-M. Wang, Nucl. Instrum. Methods: Phys. Res. B 70 (1992) 579.
[17] F.-G. Qin, X.-M. Wang, Z.-K. Liu, Zh.-Y. Yao, Zh.-Zh. Ren, L.-Y. Lin, Sh.-J. Su, W.-Sh. Jiang, W.M. Lau, Rev. Sci. Instrum. 62 (1991) 2322.
[18] M. Hong, J. Kwo, A.R. Kortan, J.P. Mannaerts, A.M. Sergent, Science 283 (1999) 1897.
[19] J. Kwo, M. Hong, A.R. Kortan, K.L. Queeney, et al., J. Appl. Phys. 89 (2001) 3920.
[20] B.D. Cullity, Elements of X-ray Diffraction, Addison-Wesley, Reading, MA, 1978, p. 411.
[21] J.-P. Zhou, D. Li, Y.-S. Gu, X.-R. Chang, Ch.-Sh. Zhao, F.-Sh. Li, L.-J. Qiao, Zh.-Zh. Tian, G.-D. Fang, Q.-Sh. Song, J. Magn. Magn. Mater. 238 (2002) L1.
[22] J.-P. Zhou, D. Li, Y.-S. Gu, X.-R. Chang, Ch.-Sh. Zhao, F.-Sh. Li, L.-J. Qiao, Zh.-Zh. Tian, G.-D. Fang, Q.-Sh. Song, IEEE Trans. Magn. 37 (2001) 3844.
[23] J.-P. Zhou, Ch.-L. Chai, Sh.-Y. Yang, Zh.-K. Liu, Sh.-L. Song, N.-F. Chen, L.-Y. Lin, J. Appl. Phys. 94 (2003) 4414.
[24] G. Van der Laan, E. Arenholz, E. Navas, A. Bauer, G. Kaindl, Phys. Rev. B 53 (1996) R5998.
[25] W.J. Lademan, A.K. See, L.E. klebanoff, G. Van der Laan, Phys. Rew. B 54 (1996) 17191.
[26] J. Szade, J. Lachnitt, M. Neumann, Phys. Rew. B 55 (1997) 1430.
[27] J.F. Moulder, et al., Handbook of X-ray Photoelectron Spectroscopy, Perkin. Elmer corp., Phys. Electr. Div., Eeden Prairie, Minnesota, 1992, p. 45 and p. 153.